



# *Ziziphus spina-christi* leaves biochar decorated with Fe<sub>3</sub>O<sub>4</sub> and SDS for sorption of chromium (III) from aqueous solution

Shima Shiraghaei Koutenaie<sup>1</sup> · Gholamhossein Vatankhah<sup>1</sup> · Hossein Esmaeili<sup>1</sup>

Received: 6 May 2022 / Revised: 27 June 2022 / Accepted: 4 July 2022 / Published online: 11 July 2022  
© The Author(s), under exclusive licence to Springer-Verlag GmbH Germany, part of Springer Nature 2022

## Abstract

The purpose of this study was to remove Cr(III) ions from aqueous solution using biochar@Fe<sub>3</sub>O<sub>4</sub>@SDS nanocomposite. Biochar@Fe<sub>3</sub>O<sub>4</sub>@SDS was synthesized as a novel adsorbent by chemical co-precipitation method. The structural features of the nanocomposite were investigated using energy-dispersive spectroscopy (EDS), dynamic light scattering (DLS), X-ray diffraction (XRD), Brunauer–Emmett–Teller (BET), Fourier transform infrared spectroscopy (FTIR), scanning electron microscopy (SEM), and transmission electron microscopy (TEM) analyses. The BET surface area and the mean pore diameter of the biochar@Fe<sub>3</sub>O<sub>4</sub>@SDS were 102.04 m<sup>2</sup>/g and 169.49 Å, respectively, indicating the high porosity of the aforementioned nanocomposite. DLS and XRD analyses showed that the mean particle size and crystal size of biochar@Fe<sub>3</sub>O<sub>4</sub>@SDS are 78.9 nm and 28 nm, respectively. Also, the highest Cr(III) removal efficiency (99.5%) using biochar@Fe<sub>3</sub>O<sub>4</sub>@SDS was obtained at pH = 9, contact time = 40 min, temperature = 55 °C, the Cr(III) ion concentration = 10 mg/L, and the nanocomposite dosage = 2 g/L. Moreover, the maximum sorption capacity obtained from the Langmuir model was 120.48 mg/g, which is a significant value compared to previous studies for Cr(III) removal. Furthermore, the isotherm study indicated that the Cr(III) sorption process using the aforementioned nanocomposite followed the Freundlich models due to the higher correlation coefficient (0.986). Also, the pseudo-second order kinetic model with a correlation coefficient of 1 was better fitted than the pseudo-first order model with experimental data. Subsequently, the thermodynamic study demonstrated that the sorption process of Cr(III) ions using biochar@Fe<sub>3</sub>O<sub>4</sub>@SDS is favorable, feasible, spontaneous, and endothermic.

**Keywords** Biochar@Fe<sub>3</sub>O<sub>4</sub>@SDS nanocomposite · Cr(III) ions · Aqueous solution · Sorption

## 1 Introduction

Water is the most important substance on earth that is used [1]. Contaminants generated by human activities such as heavy metals have severe effects on human life, animal health, and the environment [2, 3]. These contaminants are not biodegradable and cause different diseases. Chromium (Cr) is among the eleven most dangerous environmental contaminants [4–6]. Due to the high solubility of heavy metal ions in aquatic media, these metal ions may be adsorbed by living organisms. Chromium ion is considered as a highly toxic water pollutant. Chemicals industries, dyes, steelworks, leather tanning, photographic material, cement industries, and anti-corrosive paints generate high content

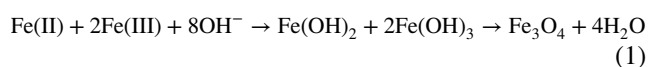
of chromium wastes [7, 8]. Though the trivalent chromium [Cr(III)] is known to be less lethal than hexavalent chromium [Cr(VI)], its removal as a water-soluble species may significantly increase public health issues because it oxidizes to [Cr(VI)] in the natural environment. Cr(III) is the predominant chromium species in the environment. The oxidation of Cr(III) to Cr(VI) by kinetically dissolved oxygen is so unfavorable at ambient temperature that chromium (III) is practically stable [9]. Exposure to excess chromium is expected to cause lung cancer and other respiratory diseases. Direct skin contacts with Cr(III) result in various issues like irritation of the skin (e.g., ulcers, rashes, and permanent scarring). Therefore, removal of Cr(III) from wastewater, if it is excessive, is of great importance [10]. According to WHO standards, the maximum allowable dosage of Cr(III) is 5 mg/L [9].

The most important approaches for eliminating metal ions from sewages and aquatic solutions include ion exchange, chemical precipitation, membrane filtration,

✉ Hossein Esmaeili  
esmaeili.hossein@gmail.com

<sup>1</sup> Department of Chemical Engineering, Bushehr Branch, Islamic Azad University, Bushehr, Iran

photocatalytic process, flocculation, electrochemical treatment, and sorption [11, 12]. Among the above procedures, sorption by nanoparticles is environment friendly, effective, simple, high selectivity, affordable, without toxic and dangerous pollutants, conveniently generalized to large scales, highly reversible technology, and is a highly efficient technology for removing metal ions [13, 14]. Activated carbon is one of the most extensively utilized sorbents in water treatment due to its high sorption capacity and good stability [13, 15]. However, the biggest problem is its higher cost than other sorbents as well as the difficulty of recovering it [15]. Finding an alternative to AC, which is both abundant and inexpensive, is an issue that has received much attention. So far, cheap and abundant natural materials such as agricultural wastes (e.g., wheat straw, seeds, wood, and fruit peel) have been utilized to fabricate biochar. Biochar produced from wheat straw [16, 17], and biochar synthesized from soy waste, algae waste, and mustard waste [18] are examples of efficient biochar with high contaminant removal efficiency. Lotus with the scientific name of *Spina-christi Ziziphus* is a plant from the family of jujube that grows wildy in Saudi Arabia, North Africa, and southern provinces of Iran. Due to the abundance and low cost of this plant, in this study, its leaves were used to generate biochar [19]. Also, iron oxide nanoparticles were used to enhance the sorbent efficiency and its recyclability. Nano-adsorbents have many applications in water and wastewater treatment because of their high active surface area, aggregation properties, high reactivity, and catalytic potential. In recent years, magnetite ( $\text{Fe}_3\text{O}_4$ ) nanoparticles have been considered in the field of water treatment; because not only it is a strong sorbent but also an active regenerator [20]. It is also easily separated from the environment by a strong magnetic field, which is useful in terms of recovery and reuse. Iron oxide comes in many forms in nature, with maghemite ( $\gamma\text{-Fe}_2\text{O}_3$ ), magnetite ( $\text{Fe}_3\text{O}_4$ ), and hematite ( $\alpha\text{-Fe}_2\text{O}_3$ ) being the most common.  $\text{Fe}_3\text{O}_4$  nano-particles are the most investigated substances because of their superparamagnetic behaviors at 25 °C. In addition, they are non-toxic and highly bio-compatible [21–23]. Furthermore, to prevent precipitation and accumulation of this nanosorbent, its surface properties were improved with sodium dodecyl sulfate (SDS), which is one of the most powerful anionic surfactants [24, 25]. The coprecipitation method maybe is the simplest and the most effective way to synthesize magnetic nanoparticles. In this procedure,  $\text{Fe}^{2+}$  and  $\text{Fe}^{3+}$  ions are stoichiometrically added to an aqueous solution and can produce superparamagnetic nanoparticles under alkaline conditions. The main reaction occurs below:



$\text{Fe}_3\text{O}_4$  can be converted to  $\gamma\text{-Fe}_2\text{O}_3$  in the presence of  $\text{H}^+$ . Therefore, to prevent adverse reactions, it is necessary to control the reaction pH along the path. Large scale-production of nanoparticles as well as controlling their size is the most important advantage of the co-precipitation method [12].

In this study, the biochar@ $\text{Fe}_3\text{O}_4$ @SDS nanocomposite was used as an efficient sorbent to eliminate Cr(III) from synthetic wastewater. The surface characterizations of biochar@ $\text{Fe}_3\text{O}_4$ @SDS were investigated by SEM, TEM, EDS, FTIR, DLS, XRD, and BET analyses. Also, the impact of temperature, pH, contact time, Cr(III) ion concentrations, and nanocomposite dosage on Cr(III) sorption was examined and the best sorption efficiency was obtained. Moreover, kinetic, equilibrium, and thermodynamic models were employed to survey the sorption behavior of the nanocomposite. To the best of our knowledge, biochar@ $\text{Fe}_3\text{O}_4$ @SDS was produced and used for the first time in this work. So far, various works have been done with iron nanoparticles and biochar, but their surface modification has not been investigated using SDS anionic surfactant. Also, surface features of biochar@ $\text{Fe}_3\text{O}_4$ @SDS were fully studied by various analyses. Moreover, the sorption capability of biochar@ $\text{Fe}_3\text{O}_4$ @SDS for Cr(III) removal was studied.

## 2 Materials and procedures

### 2.1 Chemicals and devices

$\text{FeCl}_2 \cdot 4\text{H}_2\text{O}$ ,  $\text{FeCl}_3 \cdot 6\text{H}_2\text{O}$  (Merck Company, purities > 0.99) and sodium dodecyl sulfate (SDS, Merck, purity = 0.98) were used to synthesize biochar@ $\text{Fe}_3\text{O}_4$ @SDS nanocomposite. Also, chromium trichloride hexahydrate ( $\text{CrCl}_3 \cdot 6\text{H}_2\text{O}$ , Merck, purity = 0.99) was employed to prepare chromium stock solutions. NaOH and HCl (Merck Company, purities > 0.99) were also used to regulate pH using a pH meter (Metrohm 44 model).

A flame atomic absorption device (Younglin AAS8020 model) was used to specify the remaining chromium ions in solutions. Also, a digital scale (Sartorius model) and magnetic stirrer (HS-860) were used to measure the samples weight and stir the solutions, respectively. Moreover, an oven (ATBIN MEGA model) was used to dry the biochar@ $\text{Fe}_3\text{O}_4$ @SDS nanocomposite.

### 2.2 Chromium stock solutions

To prepare chromium (III) ion stock solutions with a primary concentration of 1000 ppm, 5.12 g of  $\text{CrCl}_3 \cdot 6\text{H}_2\text{O}$  salt was dissolved in double distilled water. The stock solution

was then diluted to synthesize stock solutions at lower concentrations.

### 2.3 Preparing biochar@Fe<sub>3</sub>O<sub>4</sub>@SDS nanocomposite

Biochar@Fe<sub>3</sub>O<sub>4</sub>@SDS nanocomposite was produced by the chemical coprecipitation method. First, lotus leaves were gathered and washed several times to wipe out any dust and impurities. The leaves were then placed in an oven at 105 °C for 2 h for drying. Next, they were turned into biochar at 450 °C for 4 h. After that, the biochar was poured into a 3 M NaOH solution and stirred with a magnetic stirrer for 2 h. Then, the biochar was isolated from the suspension and dried at 105 °C for 2 h. Finally, the biochar was placed in the furnace at 700 °C for 4 to be fully activated.

To prepare biochar@Fe<sub>3</sub>O<sub>4</sub>@SDS nanocomposite, a solution containing Fe<sup>3+</sup> and Fe<sup>+2</sup> (molar ratio of 2:1) was prepared. Then, 1 g of biochar powder and 0.5 g of SDS were added to the solution at 60 °C and the suspension was stirred for 20 min at 400 rpm. Next, 3 M NaOH solution was added dropwise to the mix to make the solution black. After that, the synthesized nanocomposite was isolated from the suspension by a magnet and washed with distilled water to neutralize. Finally, the biochar@Fe<sub>3</sub>O<sub>4</sub>@SDS nanocomposite was put in the oven at 105 °C for a day to completely dry. Figure S1 shows a schematic of the synthesis of the biochar@Fe<sub>3</sub>O<sub>4</sub>@SDS nanocomposite and its use for Cr(III) removal.

To analyze the sorption features of biochar@Fe<sub>3</sub>O<sub>4</sub>@SDS nanocomposite, SEM, EDS (TESCAN, MIRA III model, Czech Republic), BET (ASAP2020, MICROMERITICS, USA), XRD (PHILIPS, PW1730, Netherlands), DLS (HORIBA, SX100, Japan), FTIR (THERMO, AVATAR, USA), EDS, and TEM (PHILIPS, CM120, Netherlands) analyses were done.

### 2.4 Sorption experiments

Sorption experiments were discontinuously done into 250-mL Erlenmeyer flasks containing 50 mL of chromium ions using biochar@Fe<sub>3</sub>O<sub>4</sub>@SDS nanocomposite. To this end, the impact of various factors on several levels was studied on the sorption process, including pH (3–11), temperature (25–55 °C), time (10–120 min), chromium (III) ion concentration (5–50 mg/l), and nanocomposite dose (0.25–5 g/L). The rate of mixing for all experiments was considered 200 rpm. After each experiment, the residual concentration of Cr(III) ions in the suspension was specified by atomic absorption spectrometry. For investigating the impact of pH, several experiments were done at various pHs (3, 5, 7, 9, and 11) while other factors were kept

constant (T = 25 °C, time = 80 min, adsorbent dose = 2 g/L, and Cr(III) concentration = 10 ppm). After performing the experiments, the best pH value was determined at the highest Cr (III) removal efficiency. Sorption efficiency (R%) and sorption capacity (q<sub>e</sub>) of biochar@Fe<sub>3</sub>O<sub>4</sub>@SDS nanocomposite can be calculated as follows:

$$\%R = \frac{(C_i - C_o)}{C_i} \times 100 \quad (2)$$

$$q_e = \frac{C_i - C_0}{M} \times V \quad (3)$$

where, C<sub>i</sub> (mg/l), C<sub>o</sub> (mg/l), M (g), and V (L) are initial concentration, Cr(III) equilibrium concentration, the nanocomposite mass, and the Cr(III) solution volume, respectively.

### 2.5 Sorption isotherms

Sorption isotherm equations are utilized to describe the equilibrium behavior of adsorbed molecules on the sorbent surface. Freundlich and Langmuir isotherms are the most important equations applied in the uptake process. The Langmuir isotherm assumes that the uptake of contaminants occurs as a mono-layer on the nanocomposite surface and there is a strong interaction between the sorbent and the adsorbed component (Eq. (4)) [26]:

$$\frac{C_e}{q_e} = \frac{C_e}{q_{max}} + \frac{1}{q_{max} K_L} \quad (4)$$

where C<sub>e</sub>, q<sub>e</sub>, K<sub>L</sub>, and q<sub>max</sub> are the equilibrium concentration of the adsorbed adsorbate (mg/L), the amount of adsorbed adsorbate per gram of the nanocomposite (mg/g), the Langmuir constant, and the utmost sorption capacity (mg/g), respectively [27]. Also, the Freundlich model assumes that the uptake of pollutants takes place on the heterogeneous surfaces of the sorbent and in multiple layers (Eq. (5)) [28]:

$$\log q_e = \log K_f + \log C_e \quad (5)$$

where n and K<sub>f</sub> are the Freundlich model constants. Also, n describes the deviation of the sorption process from linearity. For 1 < n < 10, the uptake process is physical and desirable [29].

### 2.6 Sorption kinetics

A powerful way to understand the reaction mechanism is to check the sorption kinetics. It is a critical factor in evaluating the efficiency, design, and modeling of the sorption process [27]. The most commonly used kinetic models are pseudo-first-order (PFO) and pseudo-second-order (PSO) kinetic models as defined in Eqs. (6) and (7) [26].

$$\ln(q_e - q_t) = \ln(q_e) - k_1 t \quad (6)$$

$$\frac{t}{q_t} = \frac{1}{K_2 q_e^2} + \frac{t}{q_e} \quad (7)$$

where  $q_t$ ,  $k_1$ , and  $K_2$  are the amount of adsorbed ion per gram of sorbent at time  $t$  (mg/g), the sorption rate constant of the PFO model (1/min), and the equilibrium constant of the PSO model (g/mg.min), respectively [30].

## 2.7 Sorption thermodynamic

Thermodynamic parameters are essential to specify the spontaneity of a sorption process. Thermodynamic indices for the sorption process are assessed by calculating Gibbs standard free energy variations ( $\Delta G^\circ$ ), standard enthalpy variations ( $\Delta H^\circ$ ), and standard entropy variations ( $\Delta S^\circ$ ), as described below:

$$-RT \ln(55.5K_D) = \Delta G^\circ \quad (8)$$

$$\Delta G^\circ = \Delta H^\circ - T\Delta S^\circ \quad (9)$$

where  $R$  and  $K_D$  are the universal gas constant ( $8.314 \text{ J mol}^{-1} \cdot \text{K}^{-1}$ ) and the equilibrium constant obtained from Eq. (10), respectively. Also, the number 55.5 represents the number of water moles per solution liter.

$$K_D = \frac{q_e}{C_e} \quad (10)$$

A negative value of  $\Delta G^\circ$  demonstrates the spontaneous nature of the uptake process. Absolute values between  $-20$  and  $0$  indicate physical sorption and between  $-80$  and  $-400 \text{ kJ/mol}$  mean chemical sorption [31].

$$\ln(55.5K_D) = \frac{-\Delta G^\circ}{RT} = \frac{-\Delta H^\circ}{RT} + \frac{\Delta S^\circ}{R} \quad (11)$$

## 3 Results and discussion

### 3.1 Characterization of biochar@Fe<sub>3</sub>O<sub>4</sub>@SDS

Functional groups in the structures of biochar and biochar@Fe<sub>3</sub>O<sub>4</sub>@SDS before and after uptake of Cr(III) ions were determined by FTIR analysis and outputs are illustrated in Fig. 1. In the biochar structure, an absorption peak was observed at  $454.5 \text{ cm}^{-1}$ , which is attributed to Ca-O bond. Two peaks were also seen at  $572.74$  and  $604.74 \text{ cm}^{-1}$ , which are related to Fe-O bond, while these peaks disappeared in the biochar@Fe<sub>3</sub>O<sub>4</sub>@SDS structure. The next peak appeared at  $876.05 \text{ cm}^{-1}$  related to C-H aromatic group. Two other

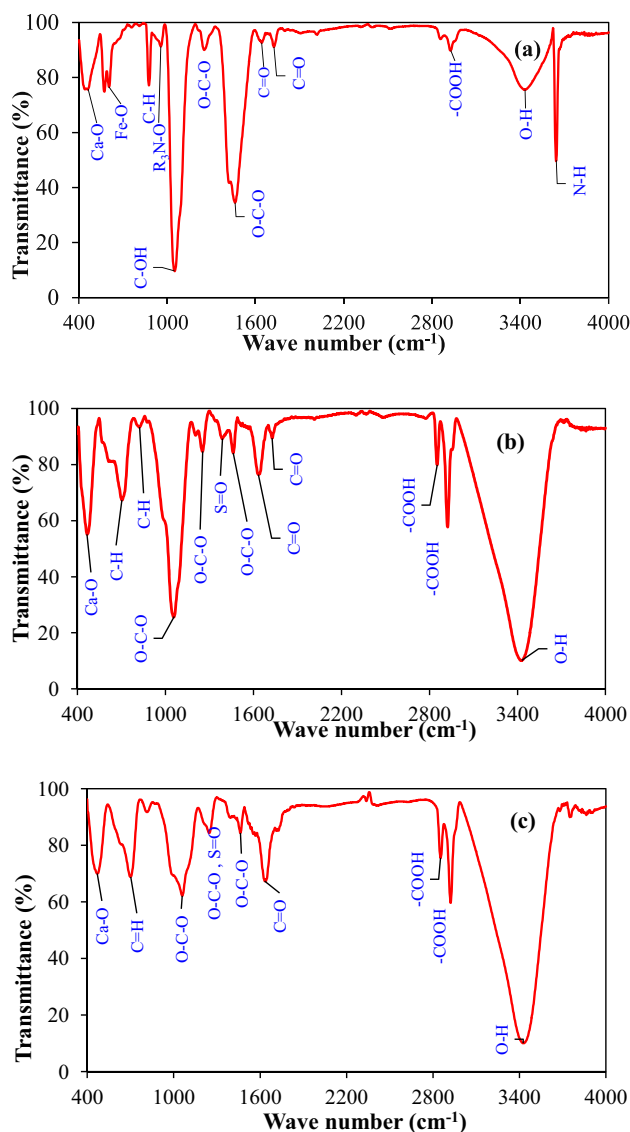


**Fig. 1** FTIR analysis for biochar (a), biochar@Fe<sub>3</sub>O<sub>4</sub>@SDS nanocomposite before uptake of chromium (b), and after uptake of chromium ions (c)

peaks at  $956.49$  and  $1050.94 \text{ cm}^{-1}$  belong to the R<sub>3</sub>N-O aliphatic and C-OH phenol groups, respectively. The R<sub>3</sub>N-O peak disappeared in the biochar@Fe<sub>3</sub>O<sub>4</sub>@SDS structure. Also, two peaks at  $1251.93$  and  $1461.36 \text{ cm}^{-1}$  belong to the O-C-O carbonate group and the two other peaks at  $1642.14$  and  $1725.51 \text{ cm}^{-1}$  belong to the C=O tensile vibration. Finally, -COOH vibration was seen at  $2925.65 \text{ cm}^{-1}$  as well as O-H and N-H vibrations were seen at  $3432.75$  and  $3643.57 \text{ cm}^{-1}$  [25, 32]. Figure 1(b) shows the FTIR spectra of biochar@Fe<sub>3</sub>O<sub>4</sub>@SDS nanocomposite before sorption. The appeared peak at  $466.87 \text{ cm}^{-1}$  belongs to the Ca-O tensile vibration, while this peak was observed in the biochar structure at  $454.5 \text{ cm}^{-1}$ . Two absorption peaks at  $704.06$  and  $822.08 \text{ cm}^{-1}$  belong to the C-H bond. Also, two

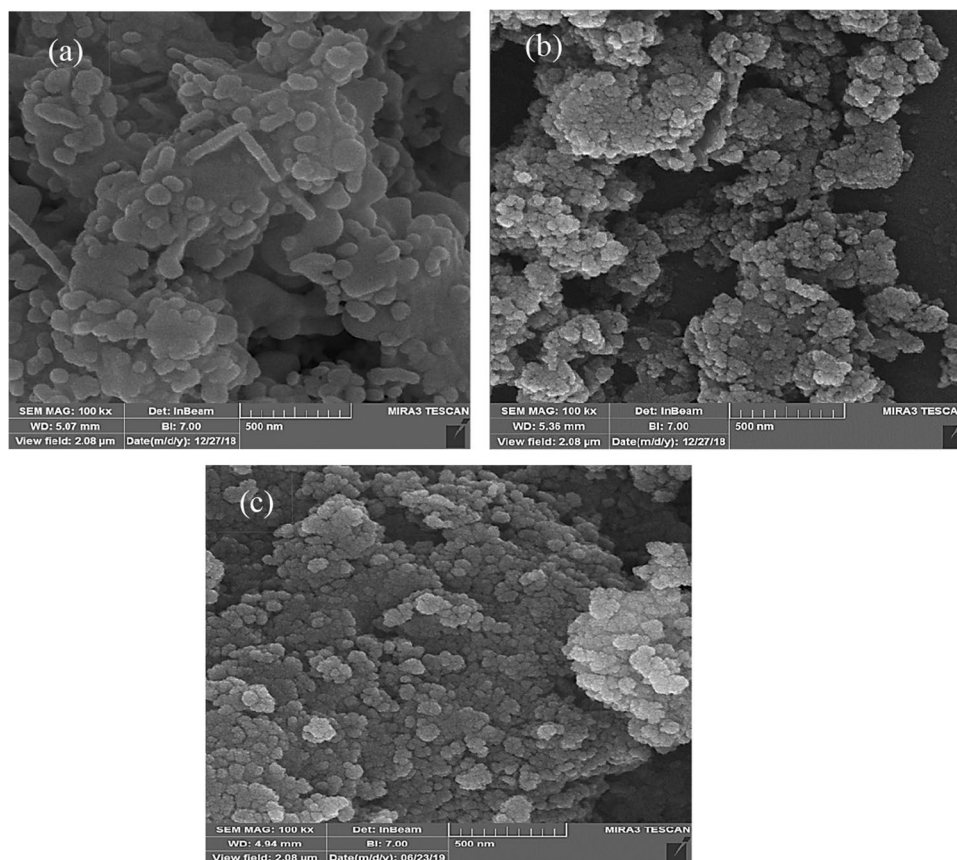
peaks at 1056.51 and 1252.21  $\text{cm}^{-1}$  are attributed to the O-C-O groups, respectively. Another peak at 1386.96  $\text{cm}^{-1}$  belongs to the asymmetric vibration bond of S=O in sulfonic acid. Moreover, a peak was seen at 1462.11  $\text{cm}^{-1}$ , which is attributed to the O-C-O carbonyl group. The O-C-O peaks in the biochar@Fe<sub>3</sub>O<sub>4</sub>@SDS structure have slightly shifted compared to biochar. Furthermore, the C=O tensile vibration was observed at 1633.47 and 1727.98  $\text{cm}^{-1}$ . Also, two other peaks at 2852.14 and 2923.31  $\text{cm}^{-1}$  belong to the -COOH functional group, which are stronger than these peaks in biochar. Also, a new and strong peak was observed at 3427.54  $\text{cm}^{-1}$ , which is attributed to the O-H hydroxyl vibration (due to the absorption of water in the nanocomposite surface). The presence of these peaks specifically O-C-O, C=O, and N-H vibrations is very important in the sorption process [25, 26]. Figure 1(c) indicates the FTIR spectra of biochar@Fe<sub>3</sub>O<sub>4</sub>@SDS nanocomposite after sorption of Cr(III). The peak at 468.86  $\text{cm}^{-1}$  belongs to the Ca-O tensile vibration. Also, C-H aromatic bond appeared at 699.64  $\text{cm}^{-1}$ . Moreover, two absorption peaks were seen at 1059.58 and 1246.84  $\text{cm}^{-1}$ , which are attributed to the O-C-O carbonate group and S=O vibration absorption in SDS, respectively. The appeared peak at 1059.58  $\text{cm}^{-1}$  is weakened compared to the nanocomposite before sorption. The appeared peak at 1462.96  $\text{cm}^{-1}$  is also related to

the O-C-O carbonate group. The C=O tensile vibration appeared at 1632.06  $\text{cm}^{-1}$ . Furthermore, absorption peaks at 2853.09 and 2922.67  $\text{cm}^{-1}$  belong to the -COOH carboxyl group and a strong peak at 3425.91  $\text{cm}^{-1}$  belongs to the O-H hydroxyl group vibration, which have slightly shifted compared to biochar@Fe<sub>3</sub>O<sub>4</sub>@SDS before sorption [32–34].

Also, for characterizing the surface morphology of biochar and biochar@Fe<sub>3</sub>O<sub>4</sub>@SDS nanocomposite before uptake of chromium (III) ions, SEM analysis was employed and outputs are demonstrated in Fig. 2. As indicated in Fig. 2(a), biochar particles have a spherical and porous structure, which indicate that biochar has a porous structure. Figure 2(b) shows that before the sorption process, there are many bumps and pores in the biochar@Fe<sub>3</sub>O<sub>4</sub>@SDS structure so that Fe<sub>3</sub>O<sub>4</sub> nanoparticles are placed inside the biochar layers and then SDS improves its surface, leading to unevenness and enhancing the nanocomposite specific surface area. The particle size in the structure of biochar@Fe<sub>3</sub>O<sub>4</sub>@SDS is smaller than biochar, which can be due to the presence of magnetite nanoparticles [35]. Also, after uptake of Cr(III), as shown in Fig. 2(c), many pores and holes in the biochar@Fe<sub>3</sub>O<sub>4</sub>@SDS surface are well covered by Cr(III) ion.

Crystalline phases in the biochar and biochar@Fe<sub>3</sub>O<sub>4</sub>@SDS nanocomposite structures were specified by XRD spectra. X-pert software was employed to draw XRD

**Fig. 2** SEM images of biochar (a), biochar@Fe<sub>3</sub>O<sub>4</sub>@SDS (b), and biochar@Fe<sub>3</sub>O<sub>4</sub>@SDS + Cr(III) (c)



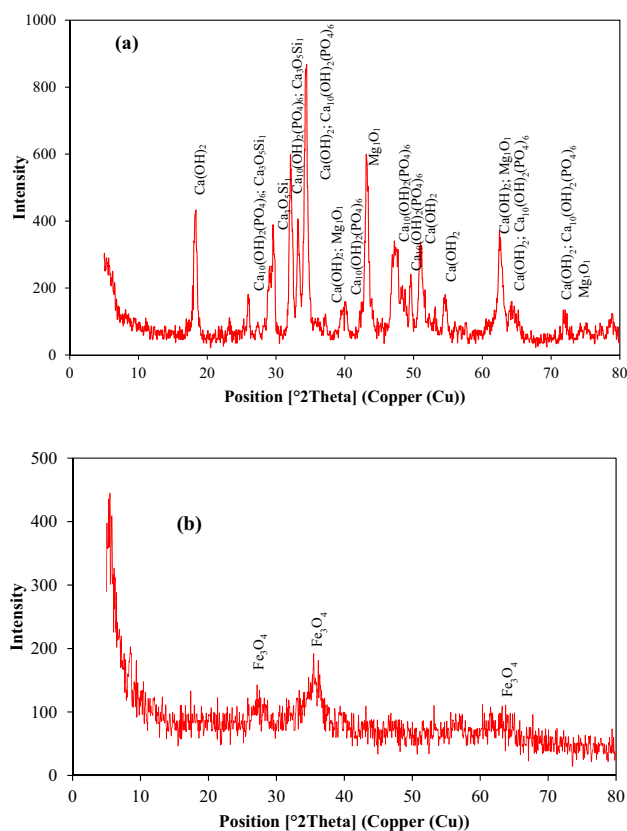


**Fig. 3** XRD patterns for biochar and biochar@Fe<sub>3</sub>O<sub>4</sub>@SDS nanocomposite

patterns and the outcomes are illustrated in Fig. 3. Several compounds such as Ca(OH)<sub>2</sub>, Ca<sub>10</sub>(OH)<sub>2</sub>(PO<sub>4</sub>)<sub>6</sub>, periclase (Mg<sub>1</sub>O<sub>1</sub>), and alite (Ca<sub>3</sub>O<sub>5</sub>Si<sub>1</sub>) were identified in the biochar structure, which are attributed to card numbers 01–076–0570, 00–001–1008, 98–006–2127, and 98–011–5657, respectively [36–38]. Also, several peaks were seen in the biochar@Fe<sub>3</sub>O<sub>4</sub>@SDS nanocomposite structure at 27, 35.5, and 63.5°, which correspond to the card number 98–001–7122 [39, 40]. The mean size of crystals was specified via  $d = \frac{K\lambda}{\beta \cos \theta}$  (Debye–Scherrer model). In this model,  $d$ ,  $\lambda$ ,  $\beta$  and  $\theta$  are the crystal size (nm), the wavelength of the apparatus (0.15406 nm), full width at half maximum, and tilt angle, respectively. Also, Scherrer constant ( $K$ ) is considered as 0.9 [32]. The mean size of crystals for biochar and biochar@Fe<sub>3</sub>O<sub>4</sub>@SDS was 217 and 28 nm, respectively.

Surface features and volume of pores for biochar and biochar@Fe<sub>3</sub>O<sub>4</sub>@SDS were specified using BET analysis (Fig. 4). The BET surface area, Langmuir surface area, the mean diameter of pores, and total volume of pores for biochar were 13.52 m<sup>2</sup>/g, 13.39 m<sup>2</sup>/g, 467.78°A, and 0.158 cm<sup>3</sup>/g, respectively. Also, these features for biochar@Fe<sub>3</sub>O<sub>4</sub>@SDS nanocomposite were 102.04 m<sup>2</sup>/g, 94.31

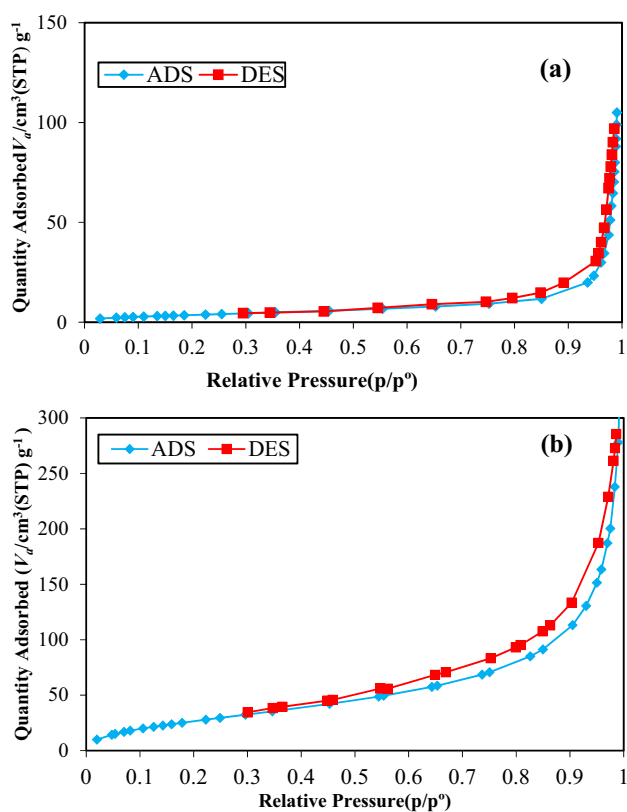


**Fig. 4** BET analyses for biochar (a) and biochar@Fe<sub>3</sub>O<sub>4</sub>@SDS (b)

m<sup>2</sup>/g, 169.49°A, and 0.432 cm<sup>3</sup>/g, respectively, indicating that the surface properties of biochar@Fe<sub>3</sub>O<sub>4</sub>@SDS nanocomposite are significantly improved compared to biochar.

Moreover, elemental compositions in the biochar@Fe<sub>3</sub>O<sub>4</sub>@SDS structure before and after uptake of Cr(III) were determined by EDS analysis (Fig. 5). Also, the percentage of elements is reported in Table 1. As shown, in the biochar@Fe<sub>3</sub>O<sub>4</sub>@SDS structure, the weight percentage of C, O, and Fe was 13.56, 43.27, and 20.54%, respectively. Also, the weight percentage of other elements such as Na, P, S, Ca, and Mg was 2.04, 5.42, 6.11, 3.73, and 5.33%, respectively. After sorption of Cr(III) using the nanocomposite, the element percentage was changed slightly. For example, the weight percentage of C, O, and Na was 18.69, 35.05, and 0.09%, respectively. Chromium also appeared with 0.16% after sorption.

Furthermore, DLS analysis was utilized to specify the particle size distribution and measure the particle size of biochar and biochar@Fe<sub>3</sub>O<sub>4</sub>@SDS composite. The outcomes are illustrated in Fig. 6 (a and b). As shown, the average particle size of biochar and biochar@Fe<sub>3</sub>O<sub>4</sub>@SDS was 81.9 and 78.9 nm, respectively. Finally, TEM analysis was employed to specify the size and morphology of

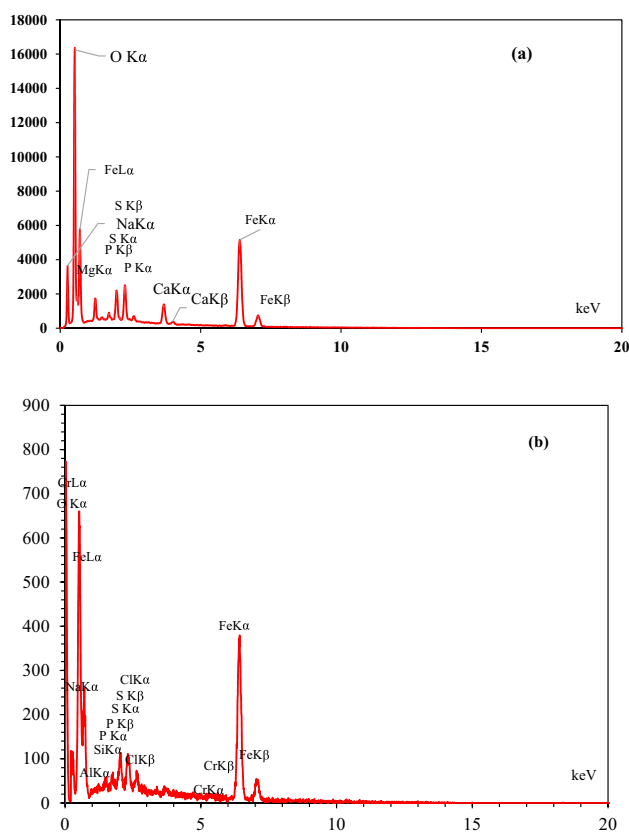


**Fig. 5** EDS analyses for biochar@Fe<sub>3</sub>O<sub>4</sub>@SDS (a) and biochar@Fe<sub>3</sub>O<sub>4</sub>@SDS + Cr(III) (b)

**Table 1** Elemental percentage in the structures of biochar@Fe<sub>3</sub>O<sub>4</sub>@SDS before and after uptake of Cr(III)

Element	Biochar@Fe <sub>3</sub> O <sub>4</sub> @SDS + Cr(III)		Biochar@Fe <sub>3</sub> O <sub>4</sub> @SDS	
	Weight per-cent (%)	Atomic percent (%)	Weight per-cent (%)	Atomic percent (%)
C	13.56	22.72	18.69	33.53
O	43.27	54.44	35.05	47.19
Na	2.04	1.79	0.09	0.09
Al	-	-	0.17	0.14
Si	-	-	0.36	0.27
P	5.42	3.52	1.45	1.01
S	6.11	3.84	1.82	1.22
Cl	-	-	0.92	0.56
Cr	-	-	0.16	0.07
Fe	20.54	7.40	41.28	15.92
Ca	3.73	1.87	-	-
Mg	5.33	4.41	-	-

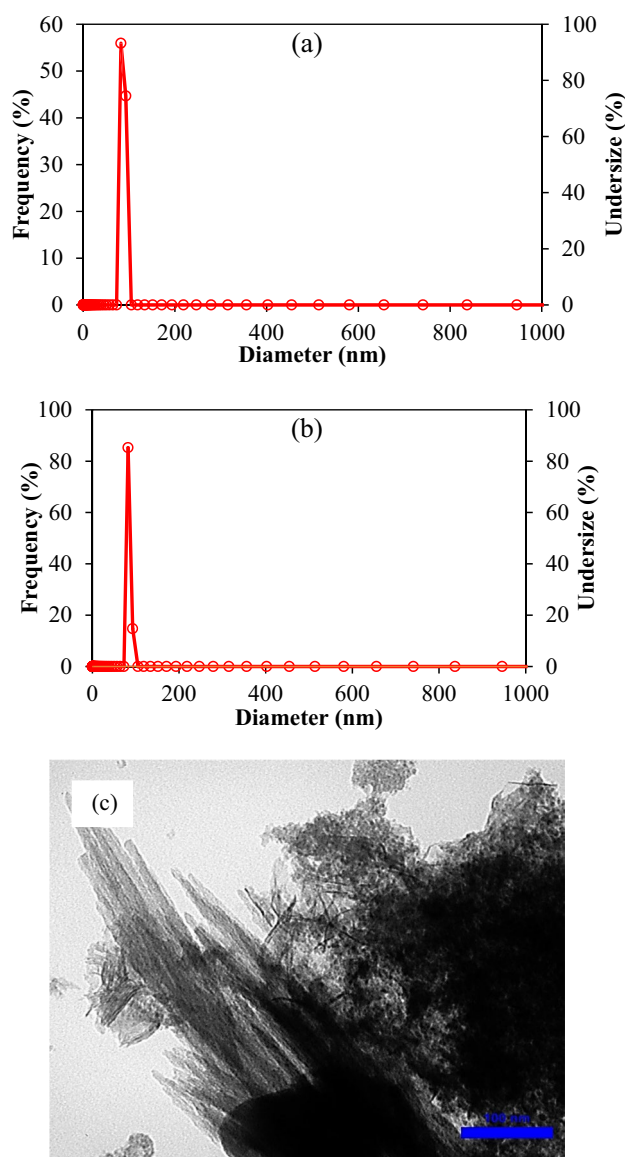


**Fig. 6** DLS analysis for biochar (a) and biochar@Fe<sub>3</sub>O<sub>4</sub>@SDS (b) and TEM analysis for biochar@Fe<sub>3</sub>O<sub>4</sub>@SDS (c)

biochar@Fe<sub>3</sub>O<sub>4</sub>@SDS. Figure 6(c) shows that the size of particles is less than 100 nm.

### 3.2 Sorption results

The initial pH of the solution has impressive impacts on the sorption process. The solution pH not only affects the surface charge of the sorbent but also affects its ionization degree [41]. The impact of pH (3–11) was studied on uptake of Cr(III) from aqueous solution using the biochar@Fe<sub>3</sub>O<sub>4</sub>@SDS nanocomposite at constant conditions like t = 80 min, Cr(III) concentration = 10 mg/L, T = 25 °C, the nanocomposite dosage = 2 g/L, and mixing rate = 200 rpm (Fig. 7(a)). At acidic pHs, the predominant forms of chromium ions are

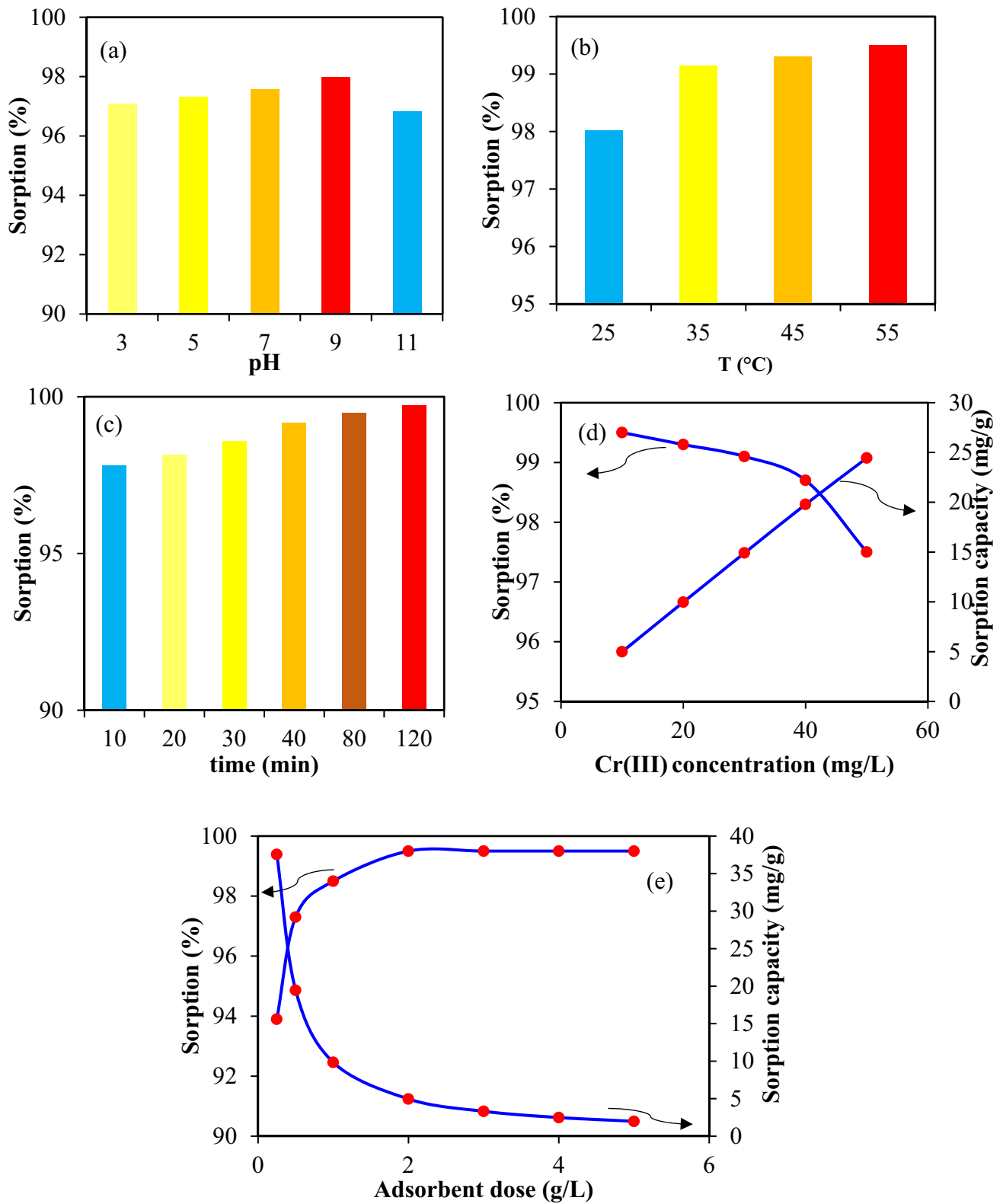


**Fig. 7** Impact of various parameters on uptake of Cr(III) using the biochar@Fe<sub>3</sub>O<sub>4</sub>@SDS nanocomposite, including pH (a), temperature (b), time (c), chromium ion concentration (d), and nanocomposite dose (e)



$\text{Cr}(\text{OH})^{2+}$ ,  $\text{Cr}^{3-}$ , and  $\text{Cr}(\text{OH})_2^+$ , which are cationic forms of Cr (III). In an alkaline environment, its hydroxide is insoluble in water. Under acidic conditions, the sorbent surface is protonated with  $\text{H}^+$  ions and as a result, the electrostatic repulsion between chromium (III) species and the nanocomposite surface reduces, ultimately leading to a decrease in the sorption efficiency. However, the concentration of protons on the nanocomposite surface reduces with increasing pH and will create a strong attraction with cationic species of chromium (III) [42, 43]. The chromium sorption efficiency enhances from 97.08 to 97.98% with increasing pH from 3 to 9, respectively, which can be due to the low concentration of  $\text{H}^+$  ions compared to Cr(III) ions for placement on the nanocomposite active sites. By raising pH from 9 to 11, the sorption efficiency reduced from 97.98 to 96.83%. At higher pHs (9–11), the  $\text{OH}^-$  concentration in the suspension is high, and these ions compete with chromium ions for placement on the nanocomposite surface, thereby reducing the sorption efficiency [44]. Therefore, pH 9 was considered as the optimal pH and at the optimal pH, the maximum sorption efficiency was 97.98%.

Temperature has an impressive impact on the sorption process because it determines whether the sorption process is endothermic and/or exothermic. The effect of temperature in the range of 25–55 °C was studied on the Cr(III) sorption efficiency by biochar@ $\text{Fe}_3\text{O}_4$ @SDS (Fig. 7(b)). To investigate the impact of temperature, other factors like pH (9), chromium (III) concentration (10 ppm), the composite dose (2 g/L), and time (80 min) were kept constant. From Fig. 7 (b), the Cr(III) sorption efficiency increases with raising the temperature so that the maximum sorption efficiency (99.5%) occurs at 55 °C, indicating that the Cr(III) sorption efficiency by biochar@ $\text{Fe}_3\text{O}_4$ @SDS is endothermic. Increasing the sorption of contaminants with increasing temperature can be due to (1) increasing the solubility of the contaminant and consequently increasing the effective contact between the adsorbent and the adsorbate (contaminant) and (2) increasing the pore size on the adsorbent surface [45]. The optimum temperature for the sorption of Cr(III) using biochar@ $\text{Fe}_3\text{O}_4$ @SDS was 55 °C.

Also, contact time is a key factor in the sorption process. The longer the contact time, the more contaminant molecules have a chance to be adsorbed on the adsorbent surface [46]. The impact of time (10–120 min) on the Cr(III) sorption efficiency by biochar@ $\text{Fe}_3\text{O}_4$ @SDS was studied at pH 9, temperature of 55 °C, the composite dose of 2 g/L, and Cr(III) concentration of 10 ppm (Fig. 7(c)). The outcomes indicate that the sorption efficiency of Cr(III) ions increases with raising time, and the sorption process includes two steps. In the first step, the Cr(III) sorption process occurred very quickly due to the high active sites of the nanocomposite. In this step, the Cr(III) sorption efficiency reached 99.18% after 40 min. However, the second step was very

slow and the Cr(III) sorption efficiency increased from 99.18 to 99.74% with enhancing time from 40 to 120 min, respectively. The active sites of the nanocomposite were gradually occupied and the sorption percentage slowly decreased [44, 47]. Hence, 40 min was considered as the optimal time.

Figure 7 (d) shows the impact of Cr(III) ions concentration on the sorption efficiency and sorption capacity using biochar@ $\text{Fe}_3\text{O}_4$ @SDS. Other factors like pH (7), contact time (40 min), temperature (55 °C), mixing speed (200 rpm), and the nanocomposite dose (2 g/L) were considered constant. As shown, the sorption capacity increases and the sorption efficiency decreases with enhancing the Cr(III) ion concentration. At low Cr(III) concentrations, there are many active sites on the nanocomposite surface that are sufficient to grab all the chromium ions. But the number of Cr(III) molecules increases at high concentrations and all of them can not be located on the active sites of the nanocomposite, thus reducing the sorption efficiency [48]. Therefore, the maximum sorption efficiency (99.5%) was achieved at a concentration of 10 mg/L Cr(III).

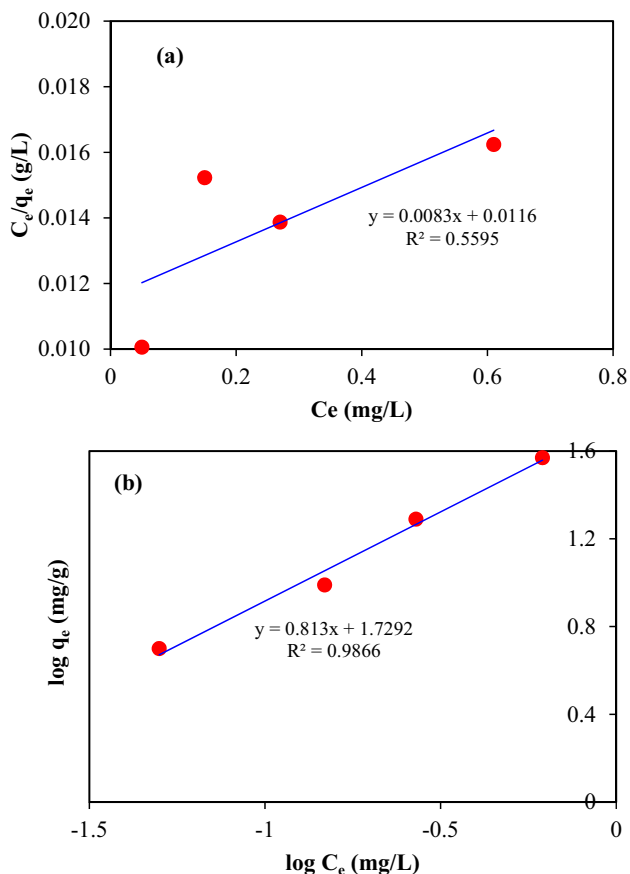
Adsorbent dosage is one of the most important factors in the sorption process because it determines the capacity of a sorbent to adsorb contaminants [6, 49]. Figure 7 (e) shows the impact of sorbent dosage (0.25–5 g/L) on uptake of Cr(III) using the biochar@ $\text{Fe}_3\text{O}_4$ @SDS nanocomposite at optimized conditions (pH=9, temperature=55 °C, time=40 min, Cr(III) concentration=10 mg/L and mixing speed=200 rpm). As demonstrated, the removal efficiency of Cr(III) increases with raising the nanocomposite dose from 0.25 to 2 g/L and at the nanocomposite dose higher than 2 g/L, the removal efficiency remained constant. Also, the sorption capacity decreased with raising the nanocomposite dose. The active sites of the nanocomposite increase with increasing sorbent dosage, which leads to more sorption of Cr(III) ions. In other words, the diffusion of Cr(III) ions into the active sites of the nanocomposite is facilitated and the sorption efficiency is increased [48]. On the other hand, increasing the nanocomposite active sites reduces the Cr(III) sorption capacity and the maximum sorption capacity was obtained at a lower sorbent dose as observed by previous studies [50]. Eventually, the highest sorption efficiency (99.5%) took place at a composite dose of 2 g/L as well as the highest sorption capacity (37.56 mg/g) took place at a composite dose of 0.25 g/L. Therefore, the optimum value of the composite dose was found to be 2 g/L.

### 3.3 Sorption isotherms of Cr(III) ions using biochar@ $\text{Fe}_3\text{O}_4$ @SDS

Sorption isotherm models describe the sorption interaction between sorbate (Cr(III)) and sorbent (Biochar@ $\text{Fe}_3\text{O}_4$ @SDS) in equilibrium state [26]. To study the sorption isotherms, several tests were done in different dosages of

**Table 2** Parameters of Langmuir (a) and Freundlich (b) models for uptake of Cr(III) using biochar@Fe<sub>3</sub>O<sub>4</sub>@SDS nanocomposite

Langmuir model				Freundlich model		
R <sub>L</sub>	K <sub>L</sub> (L/mg)	q <sub>m</sub> (mg/g)	R <sup>2</sup>	n	K <sub>f</sub> (mg/g)(mg/L) <sup>n</sup>	R <sup>2</sup>
0.123	0.71	120.48	0.559	1.23	53.6	0.986

**Fig. 8** Sorption isotherms of Langmuir (a) and Freundlich (b) for uptake of Cr(III) using biochar@Fe<sub>3</sub>O<sub>4</sub>@SDS nanocomposite

the nanocomposite (0.25–5 g/L). Other parameters were in optimized conditions (pH = 9, Cr(III) ion concentration = 10 mg/L, time = 40 min, temperature = 55 °C and mixing speed = 200 rpm). The behavior of the uptake isotherms was investigated by two known models (Langmuir and Freundlich) and outputs are reported in Table 2 and illustrated in Fig. 8. As reported, the dimensionless parameter R<sub>L</sub> was obtained at 0.123, demonstrating that the Cr(III) ions sorption process with the aforementioned nanocomposite is desirable and reversible [27]. Also, the Freundlich constant (n) was obtained at 1.23, indicating that the uptake process is favorable. Moreover, the maximum sorption capacity by the Langmuir model for the uptake of Cr(III) using the biochar@Fe<sub>3</sub>O<sub>4</sub>@SDS nanocomposite was 120.48 mg/g, which is a remarkable amount. Finally, the correlation coefficient

**Table 3** Comparing our results with previous work in the Cr(III) ion sorption

Adsorbent	q <sub>max</sub> (mg/g)	Ref
Bagasse fly ash	4.35	[52]
Coconut shell fibers AC	39.56	[53]
Modified peanut husk	3.02	[54]
Sawdust	3.34	[54]
Lignin	17.97	[55]
Graphene oxide	92.65	[56]
Rind of the <i>Jatropha curcas</i>	22.11	[57]
Endosperm of the <i>Jatropha curcas</i>	18.20	[57]
Endosperm + episperm of the <i>Jatropha curcas</i>	22.88	[57]
CaO/Fe <sub>2</sub> O <sub>3</sub>	60.60	[22]
Biochar@Fe <sub>3</sub> O <sub>4</sub> @SDS	120.48	Present study

**Table 4** Kinetic parameters for uptaking Cr(III) using biochar@Fe<sub>3</sub>O<sub>4</sub>@SDS

PSO			PFO		
q <sub>e</sub> (mg/g)	K <sub>2</sub> (g/mg.min)	R <sup>2</sup>	q <sub>e</sub> (mg/g)	K <sub>1</sub> (1/min)	R <sup>2</sup>
5	0.55	1	0.12	0.0232	0.97

(R<sup>2</sup>) indicates that the Freundlich isotherm is more proper than the Langmuir isotherm to describe the Cr(III) sorption process by biochar@Fe<sub>3</sub>O<sub>4</sub>@SDS due to its higher R<sup>2</sup>. Therefore, sorption of Cr(III) occurs in multi-layers on heterogeneous surfaces of the biochar@Fe<sub>3</sub>O<sub>4</sub>@SDS nanocomposite.

The results of this study for removing Cr(III) ions were compared with previous studies. As shown in Table 3, biochar@Fe<sub>3</sub>O<sub>4</sub>@SDS has a significant sorption capacity (120.48 mg/g) compared to other sorbents. Therefore, biochar@Fe<sub>3</sub>O<sub>4</sub>@SDS nanocomposite can be employed as a promising sorbent for industrial wastewater treatment.

### 3.4 Sorption kinetics of Cr(III) ion using biochar@Fe<sub>3</sub>O<sub>4</sub>@SDS

For investigating the kinetic behavior of Cr(III) sorption, several tests were done at the optimal pH (9), Cr(III) concentration of 10 ppm, temperature of 55 °C, a mixing speed of 200 rpm, and different times (10–120 min). To do so, the

**Fig. 9** Sorption kinetics of PFO (a) and PSO (b) for eliminating Cr(III) ions using biochar@Fe<sub>3</sub>O<sub>4</sub>@SDS nanocomposite

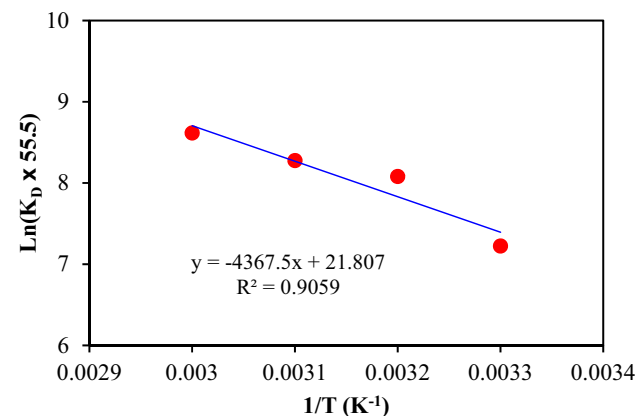
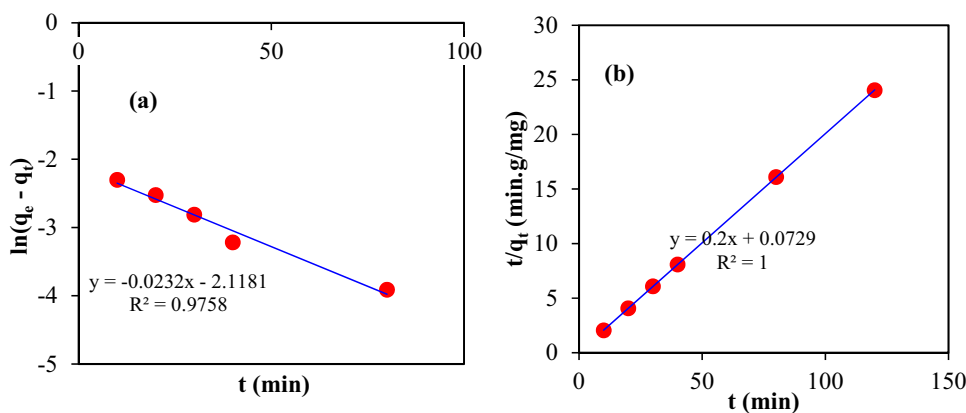


**Fig. 10** Thermodynamic investigation of Cr(III) ion sorption using biochar@Fe<sub>3</sub>O<sub>4</sub>@SDS

PFO and PSO kinetic models were utilized for fitting the laboratory data (Table 4 and Fig. 9) [51]. As reported, the value of R<sup>2</sup> for PFO and PSO models is 0.976 and 1, respectively, indicating the higher ability of the PSO model than the PFO model for sorption of Cr(III) using the biochar@Fe<sub>3</sub>O<sub>4</sub>@SDS nanocomposite. The q<sub>e</sub> calculated from the PSO model (5 mg/g) is more consistent with the laboratory data than the PFO model (0.12 mg/g). Also, the sorption rate constants of PFO (K<sub>1</sub>) and PSO (K<sub>2</sub>) models were obtained 0.0232 min<sup>-1</sup> and 0.55 g/mg.min, respectively.

**3.5 Thermodynamic investigation**

To investigate the thermodynamic behavior of the uptake process, several tests were performed at different temperatures (25–55 °C). Other factors were kept constant (pH = 9, t = 40 min, the composite dose = 2 g/L, Cr(III) concentration = 10 ppm, and mixing speed = 200 rpm). Figure 10 and Table 5 present the constants and parameters of the thermodynamic study. As reported, the amount of ΔG° for all temperatures became negative (between -17.92 and -23.52 kJ/mol) and their values are large, indicating that the Cr(III)

**Table 5** The thermodynamic parameters for uptaking Cr(III) using biochar@Fe<sub>3</sub>O<sub>4</sub>@SDS

ΔG°(kJ/mol)				ΔH°(kJ/mol)	ΔS°(J/mol.K)
298 K	308 K	318 K	328 K	36.31	181.30
-17.92	-20.70	-21.77	-23.52		

sorption process using the biochar@Fe<sub>3</sub>O<sub>4</sub>@SDS nanocomposite is spontaneous and physical. Also, the value of ΔH° is positive (36.31 kJ/mol), showing the endothermic nature of the Cr(III) sorption process using the biochar@Fe<sub>3</sub>O<sub>4</sub>@SDS nanocomposite. On the other hand, the uptake process increases with raising temperature [58, 59]. Moreover, the amount of ΔS° is positive (181.30 J/mol.K) for the Cr(III) sorption process using the biochar@Fe<sub>3</sub>O<sub>4</sub>@SDS nanocomposite, indicating an increase in randomness at the solid-solution interface is expected during the uptake process [58, 60].

**4 Conclusion**

In this study, the sorption of chromium(III) from contaminated water was studied using the biochar@Fe<sub>3</sub>O<sub>4</sub>@SDS nanocomposite. To this end, lotus leaves were utilized to prepare AC, and the nanocomposite was then synthesized by the coprecipitation process. Several analyses like TEM, EDS, DLS, XRD, BET, FTIR, and FESEM were employed to study the structural features of the aforementioned sorbent. Biochar@Fe<sub>3</sub>O<sub>4</sub>@SDS nanocomposite was synthesized and used to eliminate Cr(III) ions for the first time in this article. Different factors like pH (3–11), temperature (25–55 °C), time (10–120 min), Cr(III) ions concentration (5–50 ppm), and the nanocomposite concentration (0.25–5 g/L) were surveyed on the removal of Cr(III) ions from water using biochar@Fe<sub>3</sub>O<sub>4</sub>@SDS. According to the results, the highest sorption efficiency of Cr(III) ions was 99.5%, which was attained at pH 9, temperature of 55 °C,

Cr(III) concentration of 10 ppm, the biochar@Fe<sub>3</sub>O<sub>4</sub>@SDS dosage of 2 g/L, and time of 40 min. Also, the isotherm and kinetic studies exhibited that the Freundlich isotherm and PSO kinetic models were able to describe better the sorption process of Cr(III) ions using the biochar@Fe<sub>3</sub>O<sub>4</sub>@SDS nanocomposite because these two models had higher correlation coefficients than other isotherm and kinetic models. Moreover, the maximum sorption capacity using the biochar@Fe<sub>3</sub>O<sub>4</sub>@SDS nanocomposite was 120.48 mg/g, which is a significant value compared to previous studies for the removal of Cr(III) from aqueous solution. Furthermore, thermodynamics of the sorption process confirmed that the sorption of Cr(III) ions using the biochar@Fe<sub>3</sub>O<sub>4</sub>@SDS nanocomposite is endothermic (enthalpy change > 0), favorable and spontaneous (Gibbs free energy changes < 0). According to the results, the use of biochar@Fe<sub>3</sub>O<sub>4</sub>@SDS nanocomposite is highly recommended to remove Cr(III) ions from industrial effluents. It is also recommended that this composite be used to treat a real sample of wastewater and remove a variety of heavy metals, toxic ions, COD, BOD, and other contaminants.

**Supplementary Information** The online version contains supplementary material available at <https://doi.org/10.1007/s13399-022-03029-4>.

**Author contribution** Shima Shiraghaei Koutanaei: Conceptualization, data curation, methodology, software.

Gholamhossein Vatankhah: Conceptualization, methodology, supervision.

Hossein Esmaili: Conceptualization, Data curation and methodology. Writing-review and editing, Project administration, Validation.

**Data availability** Not applicable.

## Declarations

**Ethics approval** No approval was required. This manuscript is the authors' own original work, which has not been previously published elsewhere.

**Consent to participate** All authors contributed to this work.

**Consent for publication** All authors agree to publish.

**Competing interests** The authors declare no competing interests.

## References

- Kali A, Amar A, Loulidi I et al (2022) Characterization and adsorption capacity of four low-cost adsorbents based on coconut, almond, walnut, and peanut shells for copper removal. *Biomass Conv Bioref*. <https://doi.org/10.1007/s13399-022-02564-4>
- Zhang S, Wang J, Zhang Y et al (2021) Applications of water-stable metal-organic frameworks in the removal of water pollutants: a review. *Environ Pollut* 291:118076. <https://doi.org/10.1016/j.envpol.2021.118076>
- Zhang L, Wang L, Zhang Y et al (2022) The performance of electrode ultrafiltration membrane bioreactor in treating cosmetics wastewater and its anti-fouling properties. *Environ Res* 206:112629. <https://doi.org/10.1016/j.envres.2021.112629>
- Yu S, Tang H, Zhang D et al (2021) MXenes as emerging nanomaterials in water purification and environmental remediation. *Sci Total Environ* 811:152280. <https://doi.org/10.1016/j.scitotenv.2021.152280>
- Liu W, Huang F, Liao Y et al (2008) Treatment of Cr(VI)-Containing Mg(OH)<sub>2</sub> Nanowaste. *Angew Chem Int Ed* 47(30):5619–5622. <https://doi.org/10.1002/anie.200800172>
- Liu W, Zheng J, Ou X et al (2018) Effective extraction of Cr(VI) from hazardous gypsum sludge via controlling the phase transformation and chromium species. *Environ Sci Technol* 52(22):13336–13342. <https://doi.org/10.1021/acs.est.8b02213>
- Dai L, Wang Z, Guo T et al (2022) Pollution characteristics and source analysis of microplastics in the Qiantang River in southeastern China. *Chemosphere* 293:133576. <https://doi.org/10.1016/j.chemosphere.2022.133576>
- Liu W, Li J, Zheng J et al (2020) Different pathways for Cr(III) oxidation: implications for Cr(VI) reoccurrence in reduced chromite ore processing residue. *Environ Sci Technol* 54(19):11971–11979. <https://doi.org/10.1021/acs.est.0c01855>
- Almeida JC, Cardoso CED, Tavares DS et al (2019) Chromium removal from contaminated waters using nanomaterials – a review. *TrAC Trend Anal Chem* 118:277–291. <https://doi.org/10.1016/j.trac.2019.05.005>
- Basu A, Behera SS, Dash S et al (2019) A study on removal of Cr(III) from aqueous solution using biomass of *Cymbopogon flexuosus* immobilized in sodium alginate beads and its use as hydrogenation catalyst. *J Taiwan Inst Chem Eng* 102:118–132. <https://doi.org/10.1016/j.jtice.2019.05.012>
- Yao L, Selmi A, Esmaili H (2021) A review study on new aspects of biodemulsifiers: production, features and their application in wastewater treatment. *Chemosphere* 284:131364. <https://doi.org/10.1016/j.chemosphere.2021.131364>
- Hu M, Wang Y, Yan Z et al (2021) Hierarchical dual-nanonet of polymer nanofibers and supramolecular nanofibrils for air filtration with a high filtration efficiency, low air resistance and high moisture permeation. *J Mater Chem A* 9(24):14093–14100. <https://doi.org/10.1039/D1TA01505B>
- Qiu M, Liu L, Ling Q et al (2022) Biochar for the removal of contaminants from soil and water: a review. *Biochar* 4:19. <https://doi.org/10.1007/s42773-022-00146-1>
- Tian X, Yang R, Chen T et al (2022) Removal of both anionic and cationic dyes from wastewater using pH-responsive adsorbents of L-lysine molecular-grafted cellulose porous foams. *J Hazard Mater* 426:128121. <https://doi.org/10.1016/j.jhazmat.2021.128121>
- Rodríguez Correa C, Ngamyng C, Klank D et al (2018) Investigation of the textural and adsorption properties of activated carbon from HTC and pyrolysis carbonizates. *Biomass Conv Bioref* 8:317–328. <https://doi.org/10.1007/s13399-017-0280-8>
- Naeem MA, Imran M, Amjad M et al (2019) Batch and column scale removal of cadmium from water using raw and acid activated wheat straw biochar. *Water* 11(7):1438. <https://doi.org/10.3390/w11071438>
- Law XN, Cheah WY, Chew KW et al (2022) Microalgal-based biochar in wastewater remediation: its synthesis, characterization and applications. *Environ Res* 204:111966. <https://doi.org/10.1016/j.envres.2021.111966>
- Lucaci AR, Bulgariu D, Ahmad I (2019) Potential use of biochar from various waste biomass as biosorbent in Co (II) removal processes. *Water* 11(8):1565. <https://doi.org/10.3390/w11081565>
- Abshirini Y, Foroutan R, Esmaili H (2019) Cr (VI) removal from aqueous solution using activated carbon prepared from *Ziziphus*

- spina-christi leaf. *Mater Res Express* 6(4):045607. <https://doi.org/10.1088/2053-1591/aafb45>
20. Lucaci AR, Bulgariu D, Bulgariu L (2021) In situ functionalization of iron oxide particles with alginate: a promising biosorbent for retention of metal ions. *Polymers* 13(20):3554. <https://doi.org/10.3390/polym13203554>
  21. Liu X, Pang H, Liu X et al (2021) Orderly porous covalent organic frameworks-based materials: superior adsorbents for pollutants removal from aqueous solutions. *The Innovation* 2(1):100076. <https://doi.org/10.1016/j.xinn.2021.100076>
  22. Keshavarz M, Foroutan R, Papari F et al (2021) Synthesis of CaO/Fe<sub>2</sub>O<sub>3</sub> nanocomposite as an efficient nano-adsorbent for the treatment of wastewater containing Cr (III). *Sep Sci Technol* 56(8):1328–1341. <https://doi.org/10.1080/01496395.2020.1778727>
  23. Shi C, Wu Z, Yang F, Tang Y (2021) Janus particles with pH switchable properties for high-efficiency adsorption of PPCPs in water. *Solid State Sci* 119:106702. <https://doi.org/10.1016/j.solidstatesciences.2021.106702>
  24. Sobhanardakani S, Zandipak R, Cheraghi M (2016) Synthesis of DNPH/SDS/Fe<sub>3</sub>O<sub>4</sub> nanoparticles for removal of Cr (VI) ions from aqueous solution. *Avicenna J Environ Health Eng* 3(1):1–9. <https://doi.org/10.17795/ajehe-7789>
  25. Tamjidi S, Esmaili H (2019) Chemically modified CaO/Fe<sub>3</sub>O<sub>4</sub> nanocomposite by sodium dodecyl sulfate for Cr (III) removal from water. *Chem Eng Technol* 42(3):607–616. <https://doi.org/10.1002/ceat.201800488>
  26. Esmaili H, Tamjidi S (2020) Ultrasonic-assisted synthesis of natural clay/Fe<sub>3</sub>O<sub>4</sub>/graphene oxide for enhance removal of Cr (VI) from aqueous media. *Environ Sci Pollut Res* 27(25):31652–31664. <https://doi.org/10.1007/s11356-020-09448-y>
  27. Awual MR (2015) A novel facial composite adsorbent for enhanced copper (II) detection and removal from wastewater. *Chem Eng J* 266:368–375. <https://doi.org/10.1016/j.cej.2014.12.094>
  28. Awual MR (2019) Efficient phosphate removal from water for controlling eutrophication using novel composite adsorbent. *J Clean Prod* 228:1311–1319. <https://doi.org/10.1016/j.jclepro.2019.04.325>
  29. Veloso CH, Filippova IV, Ouvrard S, Araujo AC (2020) Adsorption of polymers onto iron oxides: equilibrium isotherms. *J Mater Res Technol* 9(1):779–788. <https://doi.org/10.1016/j.jmrt.2019.11.018>
  30. Kabir MM, Akter MM, Khandaker S et al (2022) Highly effective agro-waste based functional green adsorbents for toxic chromium (VI) ion removal from wastewater. *J Mol Liq* 347:118327. <https://doi.org/10.1016/j.molliq.2021.118327>
  31. Rambabu K, Thanigaivelan A, Bharath G et al (2021) Biosorption potential of Phoenix dactylifera coir wastes for toxic hexavalent chromium sequestration. *Chemosphere* 268:128809. <https://doi.org/10.1016/j.chemosphere.2020.128809>
  32. Sheikh TA, Rahman MM, Asiri AM et al (2018) 4-Hexylresorcinol sensor development based on wet-chemically prepared Co<sub>3</sub>O<sub>4</sub>@Er<sub>2</sub>O<sub>3</sub> nanorods: a practical approach. *J Ind Eng Chem* 66:446–455. <https://doi.org/10.1016/j.jiec.2018.06.012>
  33. Silva VAJ, Andrade PL, Silva MPC et al (2013) Synthesis and characterization of Fe<sub>3</sub>O<sub>4</sub> nanoparticles coated with fucan polysaccharides. *J Magn Magn Mater* 343:138–143. <https://doi.org/10.1016/j.jmmm.2013.04.062>
  34. Burks T, Avila M, Akhtar F et al (2014) Studies on the adsorption of chromium(VI) onto 3-Mercaptopropionic acid coated superparamagnetic iron oxide nanoparticles. *J Colloid Interface Sci* 425:36–43. <https://doi.org/10.1016/j.jcis.2014.03.025>
  35. Takmil F, Esmaili H, Mousavi SM et al (2020) Nano-magnetically modified activated carbon prepared by oak shell for treatment of wastewater containing fluoride ion. *Adv Powder Technol* 31(8):3236–3245. <https://doi.org/10.1016/j.apt.2020.06.015>
  36. Pontremoli C, Boffito M, Fiorilli S et al (2018) Hybrid injectable platforms for the in situ delivery of therapeutic ions from mesoporous glasses. *Chem Eng J* 340:103–113. <https://doi.org/10.1016/j.cej.2018.01.073>
  37. Zhang P, Hao M, Mao X et al (2020) Effects of W<sup>6+</sup> substitution on crystal structure and microwave dielectric properties of Li<sub>3</sub>Mg<sub>2</sub>NbO<sub>6</sub> ceramics. *Ceram Int* 46(13):21336–21342. <https://doi.org/10.1016/j.ceramint.2020.05.229>
  38. Yan W, Cao M, Fan S et al (2021) Multi-yolk ZnSe/(CoSe<sub>2</sub>)@NC heterostructures confined in N-doped carbon shell for high-efficient sodium-ion storage. *Compos B Eng* 213:108732. <https://doi.org/10.1016/j.compositesb.2021.108732>
  39. Faiyas APA, Vinod EM, Joseph J et al (2010) Dependence of pH and surfactant effect in the synthesis of magnetite (Fe<sub>3</sub>O<sub>4</sub>) nanoparticles and its properties. *J Magn Magn Mater* 322(4):400–404. <https://doi.org/10.1016/j.jmmm.2009.09.064>
  40. Fu Y, Chen H, Guo R (2021) Extraordinary strength-ductility in gradient amorphous structured Zr-based alloy. *J Alloys Compd* 888:161507. <https://doi.org/10.1016/j.jallcom.2021.161507>
  41. Awual MR (2019) Mesoporous composite material for efficient lead (II) detection and removal from aqueous media. *J Environ Chem Eng* 7(3):103124. <https://doi.org/10.1016/j.jece.2019.103124>
  42. Wanliang Z, Manli Z, Hongying C et al (2016) Experimental study on cleaning and detoxification of chromium in construction waste. *Procedia Environ Sci* 31:247–254. <https://doi.org/10.1016/j.proenv.2016.02.033>
  43. Awual MR (2019) Novel ligand functionalized composite material for efficient copper (II) capturing from wastewater sample. *Compos B Eng* 172:387–396. <https://doi.org/10.1016/j.compositesb.2019.05.103>
  44. Bajjnath L, Gautam V, Yadav V (2014) A comparative study of the removal efficiency of calcium hydroxide and sodium hydroxide as precipitating agents for chromium (III). *J Civ Eng Environ Technol* 1(1):17–20
  45. Manirethan V, Raval K, Rajan R et al (2018) Kinetic and thermodynamic studies on the adsorption of heavy metals from aqueous solution by melanin nanopigment obtained from marine source: *Pseudomonas stutzeri*. *J Environ Manage* 214:315–324. <https://doi.org/10.1016/j.jenvman.2018.02.084>
  46. Hasan MM, Shenashen MA, Hasan MN et al (2021) Natural biodegradable polymeric bioadsorbents for efficient cationic dye encapsulation from wastewater. *J Mol Liq* 323:114587. <https://doi.org/10.1016/j.molliq.2020.114587>
  47. Chowdhury MF, Khandaker S, Sarker F et al (2020) Current treatment technologies and mechanisms for removal of indigo carmine dyes from wastewater: a review. *J Mol Liq* 318:114061. <https://doi.org/10.1016/j.molliq.2020.114061>
  48. Panda H, Tiadi N, Mohanty M, Mohanty C (2017) Studies on adsorption behavior of an industrial waste for removal of chromium from aqueous solution. *S Afr J Chem Eng* 23:132–138. <https://doi.org/10.1016/j.sajce.2017.05.002>
  49. Xu D, Liu J, Ma T et al (2022) Coupling of sponge fillers and two-zone clarifiers for granular sludge in an integrated oxidation ditch. *Environ Technol Innov* 26:102264. <https://doi.org/10.1016/j.eti.2021.102264>
  50. Munjur HM, Hasan MN, Awual MR et al (2020) Biodegradable natural carbohydrate polymeric sustainable adsorbents for efficient toxic dye removal from wastewater. *J Mol Liq* 319:114356. <https://doi.org/10.1016/j.molliq.2020.114356>
  51. Zhao J, Liu J, Wang W et al (2016) Highly efficient removal of bivalent heavy metals from aqueous systems by magnetic porous Fe<sub>3</sub>O<sub>4</sub>-MnO<sub>2</sub>: Adsorption behavior and process study. *Chem Eng J* 304:737–746. <https://doi.org/10.1016/j.cej.2016.07.003>

52. Gupta VK, Ali I (2004) Removal of lead and chromium from wastewater using bagasse fly ash—a sugar industry waste. *J Colloid Interface Sci* 271(2):321–328. <https://doi.org/10.1016/j.jcis.2003.11.007>
53. Mohan D, Singh KP, Singh VK (2006) Trivalent chromium removal from wastewater using low cost activated carbon derived from agricultural waste material and activated carbon fabric cloth. *J Hazard Mater* 135(1–3):280–295. <https://doi.org/10.1016/j.jhazmat.2005.11.075>
54. Li Q, Zhai J, Zhang W et al (2007) Kinetic studies of adsorption of Pb(II), Cr(III) and Cu(II) from aqueous solution by sawdust and modified peanut husk. *J Hazard Mater* 141(1):163–167. <https://doi.org/10.1016/j.jhazmat.2006.06.109>
55. Wu Y, Zhang S, Guo X, Huang H (2008) Adsorption of chromium(III) on lignin. *Bioresour Technol* 99(16):7709–7715. <https://doi.org/10.1016/j.biortech.2008.01.069>
56. Yang S, Li L, Pei Z et al (2014) Adsorption kinetics, isotherms and thermodynamics of Cr(III) on graphene oxide. *Colloids Surf A Physicochem Eng Asp* 457:100–106. <https://doi.org/10.1016/j.colsurfa.2014.05.062>
57. Gonçalves AC, Nacke H, Schwantes D et al (2017) Adsorption mechanism of chromium (III) using biosorbents of *Jatropha curcas* L. *Environ Sci Pollut Res* 24(27):21778–21790. <https://doi.org/10.1007/s11356-017-9749-z>
58. Singh NB, Nagpal G, Agrawal S (2018) Water purification by using adsorbents: a review. *Environ Technol Innov* 11:187–240. <https://doi.org/10.1016/j.eti.2018.05.006>
59. Rambabu K, Bharath G, Banat F, Show PL (2020) Biosorption performance of date palm empty fruit bunch wastes for toxic hexavalent chromium removal. *Environ Res* 187:109694. <https://doi.org/10.1016/j.envres.2020.109694>
60. Yegane Badi M, Azari A, Pasalari H et al (2018) Modification of activated carbon with magnetic Fe<sub>3</sub>O<sub>4</sub> nanoparticle composite for removal of ceftriaxone from aquatic solutions. *J Mol Liq* 261:146–154. <https://doi.org/10.1016/j.molliq.2018.04.019>

**Publisher's note** Springer Nature remains neutral with regard to jurisdictional claims in published maps and institutional affiliations.